

Predicting the Rossby number in convective experiments

EVAN H. ANDERS,^{1,2} CATHRYN M. MANDUCA,² BENJAMIN P. BROWN,^{1,2} JEFFREY S. OISHI,³ AND GEOFF VASIL⁴

¹*Dept. Astrophysical & Planetary Sciences, University of Colorado – Boulder, Boulder, CO 80309, USA*

²*Laboratory for Atmospheric and Space Physics, Boulder, CO 80303, USA*

³*Department of Physics and Astronomy, Bates College, Lewiston, ME 04240, USA*

⁴*University of Sydney School of Mathematics and Statistics, Sydney, NSW 2006, Australia*

(Received September 24, 2018; Revised ??; Accepted ??)

Submitted to ApJ

ABSTRACT

In this letter we study numerical simulations of stratified, compressible convection in a rotational f -plane geometry. We define a new quantity, the Predictive Rossby number (\mathcal{P}_{Ro}), and show that it specifies the evolved rotational constraint of simulation as measured by the Rossby number (Ro). We examine the scaling of traditional fluid numbers and boundary layers along paths of constant \mathcal{P}_{Ro} .

Keywords: convection — rotation — turbulence

1. INTRODUCTION

Rotation influences the dynamics of convective flows in stellar and planetary atmospheres. An abundance of studies into the fundamental nature of rotating convection in both laboratory and numerical settings have provided great insight into the properties of convection in both the rapidly rotating regime (Julien et al. 2012; Stellmach et al. 2014; Gastine et al. 2016) and the rotationally unconstrained regime (King et al. 2009; Zhong et al. 2009; Cheng et al. 2015). The scaling behavior of heat transport, the nature of convective flow structures, and the importance of boundary layers in driving dynamics are well known, and yet we authors are not aware of a well-developed procedure for specifying the significance of rotation on the evolved convective flows in the experimental initial conditions. The importance of rotation on convective dynamics, measured by the evolved Rossby number (Ro , the ratio of convective to rotational vorticity), is in general not held constant in parameter space studies and is often not even reported.

In the astrophysical context, many studies of rotating convection have investigated questions inspired by the solar dynamo (Glatzmaier & Gilman 1982; Busse 2002; Brown et al. 2008, 2010, 2011; Augustson et al. 2012;

Guerrero et al. 2013; Käpylä et al. 2014). Even when these simulations nominally rotate at the solar rate, they frequently produce distinctly different behaviors than the true Sun, such as anti-solar differential rotation profiles. These unphysical results may arise from the fact that Ro in these simulations differs from its value the Sun. Recent simulations and experiments predict that Ro in the deep solar interior is very small, implying that deep solar convection is highly rotationally constrained, and this likely drastically affects the behavior of solar convection (Featherstone & Hindman 2016; Greer et al. 2016). In the planetary context, the balance between Lorentz and rotational forces likely leads to the observed differences between ice giant and gas giant dynamos in our solar system (Soderlund et al. 2015). Aurnou & King (2017) suggest that many studies in planetary systems have likely over-emphasized the importance of magnetism compared to rotation.

In short, simulations must have flows at the proper Rossby number if they are to have any hope of explaining the behavior of astrophysical objects. In this letter, our goal is to experimentally explore methods of specifying the Rossby number of convection in a simplified system. In Anders & Brown (2017) (hereafter AB17), we studied non-rotating, hydrodynamic, compressible convection in polytropic atmospheres. In this work, we extend the study of AB17 to rotationally-influenced, f -plane atmospheres, as have been previously studied by e.g., Brummell et al. (1996, 1998); Calkins et al. (2015). Our

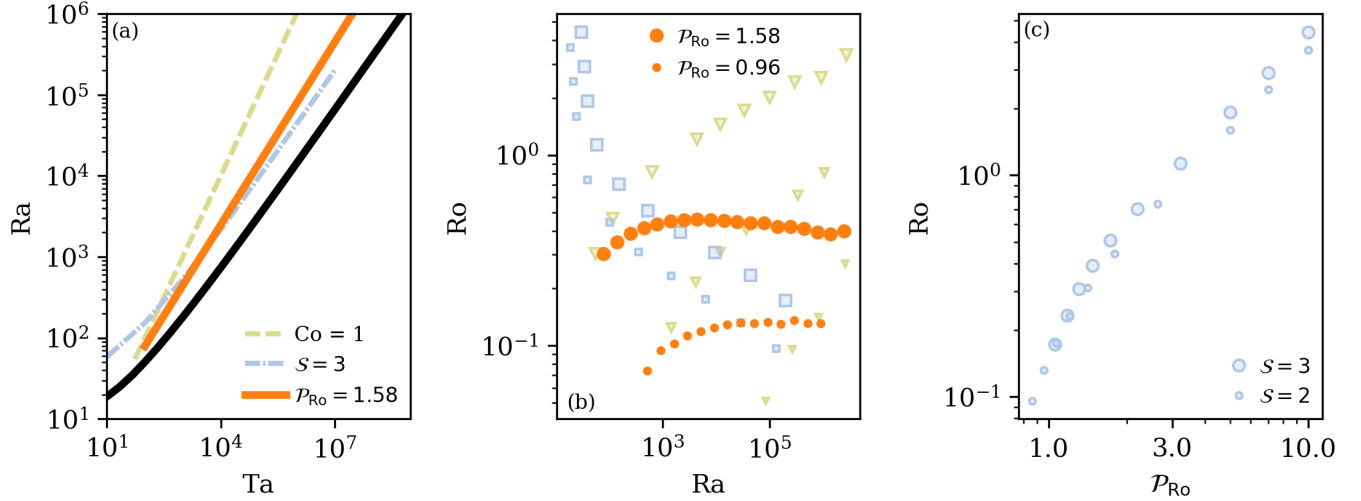


Figure 1. (a) The critical Rayleigh number, as a function of the Taylor number, is plotted as a solid black line. Paths of constant Convective Rossby Number (Co , green dashed line), constant supercriticality (S , blue dash-dot line), and \mathcal{P}_{Ro} (orange solid line) are shown through parameter space. (b) Evolved Ro is plotted vs. Ra along multiple constant \mathcal{P}_{Ro} paths. For comparison, paths of constant S (blue squares; $S = 3$ for big squares and $S = 2$ for small squares) and constant Co (green triangles; $Co = 1$ for big triangles, $Co = 0.3$ for medium triangles, and $Co = 0.1$ for small triangles) are shown. Ro is roughly constant for a constant \mathcal{P}_{Ro} , but changes drastically at constant Co and S . (c) The scaling of Ro with \mathcal{P}_{Ro} is shown for $S = (2, 3)$. At low Ro , both supercriticalities collapse onto a common scaling law of [NEED LAW]. At higher Ro , a different scaling law of [NEED LAW] is seen, and different supercriticalities shift Ro .

goal is to determine how the input parameters which we studied previously (which control the Mach number and Reynolds number of the evolved flows) couple with a new input parameter, the Taylor number (Ta , Julien et al. (1996)), which sets the magnitude of the rotational vector.

In section 2, we describe our experiment and paths through parameter space. In section 3, we present the results of our experiments and in section 4 we offer concluding remarks.

2. EXPERIMENT

We study fully compressible, stratified convection under precisely the same atmospheric model as we previously did in AB17, but here we have included rotation. We study polytropic atmospheres with $n_\rho = 3$ density scale heights and a superadiabatic excess of $\epsilon = 10^{-4}$ such that flows are at low Mach number. As in previous work (Julien et al. 1996; Brummell et al. 1996), we study a domain in which the gravity, $\mathbf{g} = -g\hat{z}$, and rotational vector, $\mathbf{\Omega} = \Omega\hat{z}$, are antiparallel.

We evolve the velocity (\mathbf{u}), temperature (T), and log density ($\ln \rho$) according to the Fully Compressible Navier-Stokes equations in the same form presented in AB17, with the addition of the Coriolis term, $2\mathbf{\Omega} \times \mathbf{u}$, to the left-hand side of the momentum equation. We impose impenetrable, stress-free, fixed-temperature

boundary conditions at the top and bottom of the domain.

The kinematic viscosity (ν), thermal diffusivity (χ), and strength of rotation (Ω) are set at the top of the domain by the Rayleigh number (Ra), Prandtl number (Pr), and Taylor number (Ta),

$$Ra = \frac{gL_z^3 \Delta S / c_P}{\nu \chi}, \quad Pr = \frac{\nu}{\chi}, \quad Ta = \left(\frac{2\Omega L_z^2}{\nu} \right)^2, \quad (1)$$

where L_z is the depth of the domain, $\Delta S = \epsilon n_\rho / m$ is the specific entropy difference between $z = 0$ and $z = L_z$, and the specific heat at constant pressure is c_P . Throughout this work we set $Pr = 1$.

As Ta increases, the wavenumber of convective onset, k_{crit} , also increases (Calkins et al. 2015). We study 3D cartesian convective domains with horizontal extents of $x, y = [0, 4(2\pi/k_{crit})]$. We evolve our simulations using the Dedalus¹ pseudospectral framework, and our numerical methods are identical to those presented in AB17.

As Ta increases, the critical value of Ra at which convection onsets, Ra_{crit} , also increases (see the black line in Fig. 1a). The linked nature of these crucial control parameters makes it difficult to predict the rotational constraint of the evolved fluid flows for a given set of input parameters. In this work, we will explore three

¹ <http://dedalus-project.org/>

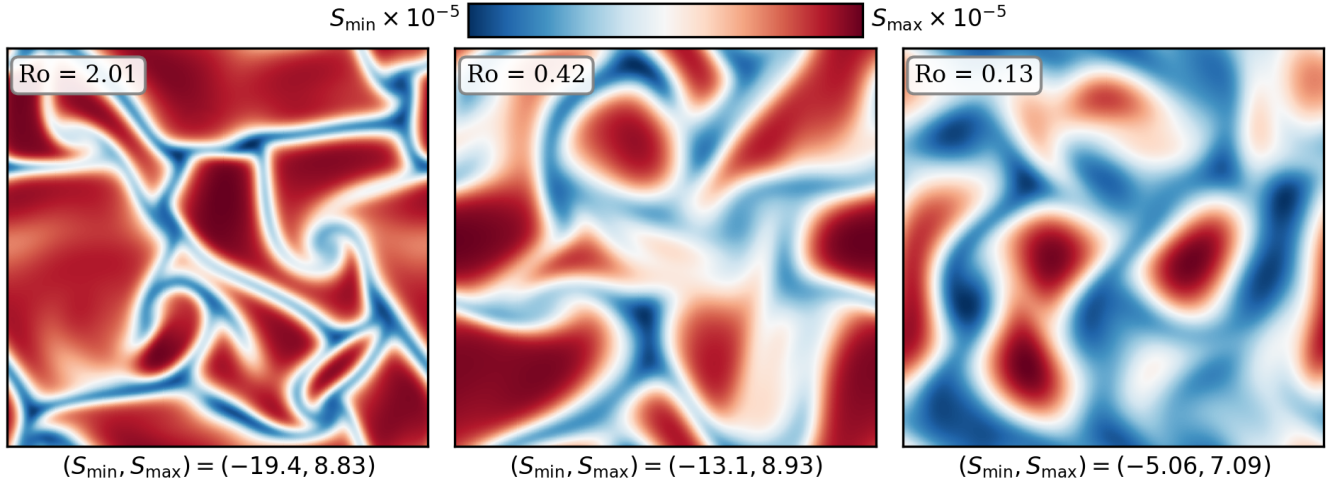


Figure 2. A horizontal slice of the evolved entropy field is plotted at $z = 0.95L_z$ for select simulations. The mean value of entropy at this height has been removed in all cases. All runs displayed here have an evolved volume-averaged $Re \sim 200$. As Ro decreases from $O(1)$ on the left to $O(0.1)$ on the right, and thus the rotational constraint on the flow increases, significant changes in flow morphology are observed. At $Ro = 2.01$, convective dynamics are not hugely dissimilar from the non-rotating case where there are large upflows and narrow, fast downflow lanes (see e.g., AB17). As the rotational constraint increases, the granular convective pattern gives way to vortical columns, as seen at $Ro = 0.13$.

paths through Ra-Ta space:

$$Ra = \begin{cases} S Ra_{\text{crit}}(Ta), & \text{(I)} \\ Co^2 Pr Ta, & \text{(II)} \\ \mathcal{P}_{Ro}^2 Pr Ta^{3/4} & \text{(III).} \end{cases} \quad (2)$$

Paths on constraint I are at constant supercriticality, $S \equiv Ra/Ra_{\text{crit}}$ (blue dash-dot line in Fig. 1a). Paths on constraint II are at a constant value of the classic “Convective Rossby number” ($Co^2 = Ra / [Pr Ta]$), which has been used frequently in past work, and is intended to predict the Rossby number of the evolved solution (green dashed line in Fig. 1a; Julien et al. (1996); Brummell et al. (1996)). Paths on constraint III set constant a ratio which we call the “Predictive Rossby Number,” $\mathcal{P}_{Ro}^2 = Ra/(PrTa^{3/4})$, (e.g., orange solid line in Fig. 1a). To our knowledge, these paths have not been explored in the literature.

For each path defined in Eqn. 2, our goal is to study the magnitude, and variation as a function of Ta , of the Rossby number,

$$Ro = \frac{|\nabla \times \mathbf{u}|}{2\Omega}, \quad (3)$$

which quantifies the degree to which the fluid is rotationally constrained.

3. RESULTS

In Fig. 1a, the value of Ra_{crit} is shown as a function of Ta , as calculated by a linear instability analysis. A sam-

ple path for each criterion in Eqn. 2 through this parameter space is shown. In Fig. 1b, we display the scaling of Ro with increasing Ra along various paths through parameter space. We find that Ro increases on constant Co paths, decreases on constant S paths, and remains roughly constant along constant \mathcal{P}_{Ro} paths. In Fig. 1c, the behavior of Ro is shown as a function of \mathcal{P}_{Ro} at constant S . At low Ro and \mathcal{P}_{Ro} , in the rotationally constrained regime, the two parameters are related according to the power law [INSERT HERE ONCE MORE DATA]. At higher Ro in the rotationally unconstrained regime, this scaling breaks down to a [INSERT SCALING], with some offset at different values of S .

In Fig. 2, sample snapshots of the evolved entropy field in the $x-y$ plane near the top of the domain are shown. In the left panel is a rotationally unconstrained flow at moderately high Ro , and Ro decreases into the rotationally constrained regime from left to right. As Ro decreases, the classic granular structure of convection (see e.g., Fig. 2 in AB17) gives way to vortical columns of convection, as seen in rapidly rotating Rayleigh-Bénard convection (Stellmach et al. 2014). The select cases displayed in Fig. 2 have an evolved volume-averaged $Re \sim 200$.

We measure the Nusselt number (Nu , which quantifies heat transport in a convective solution) as we did in AB17. In Fig. 3a, we show how Nu scales as a function of Ra at fixed \mathcal{P}_{Ro} . When $Ro \sim 0.1$, we find a scaling of $Nu \propto Ra^{0.27}$. This is reminiscent of classic scaling laws (e.g., $Ra^{2/7}$) in non-rotating Rayleigh-Bénard

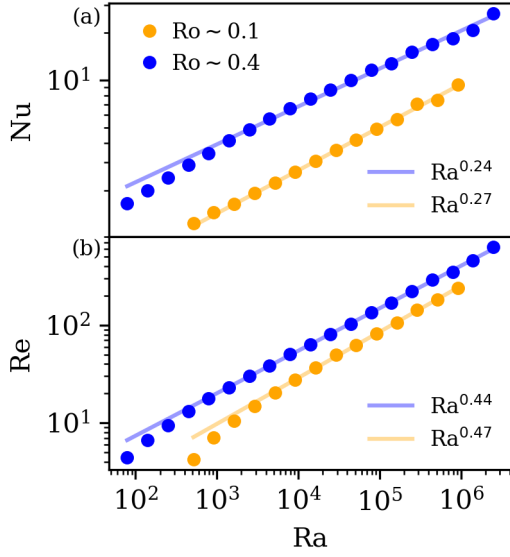


Figure 3. Scaling laws for paths at $\mathcal{P}_{\text{Ro}} = 1.58$ ($\text{Ro} \sim 0.4$) and $\mathcal{P}_{\text{Ro}} = 0.96$ ($\text{Ro} \sim 0.1$) are shown. (a) Evolved Nu vs. Ra . The scaling laws here are very reminiscent of classic Rayleigh-Bénard convection theory (Ahlers et al. 2009). (b) Evolved Re vs. Ra . The scaling seen here is nearly identical to scalings in nonrotating convection.

convection (Ahlers et al. 2009). This suggests that changes in heat transport at constant \mathcal{P}_{Ro} are driven by changes in the boundary layer structure with increasing Ra . In Fig. 3b, we plot the RMS Reynold’s number ($\text{Re} = |u|L_z/\nu$) as a function of Ra at fixed \mathcal{P}_{Ro} , and find that $\text{Re} \propto \text{Ra}^{0.47} \sim \text{Ra}^{1/2}$ in the rotationally constrained regime, which directly parallels the non-rotating regime in AB17.

In Fig. 4, we show time- and horizontally-averaged profiles of Ro and the entropy gradient (∇s). As Ra increases at a constant value of \mathcal{P}_{Ro} , both the ∇s and Ro boundary layers become thinner. We measure the thickness of the entropy boundary layer ($\delta_{\nabla s}$) at the top of the domain by measuring where a linear fit within the boundary layer crosses through $\nabla s = 0$. We ensure by-eye for each profile that this is a reasonable measure of the boundary layer thickness. We measure the thickness of the Ro boundary layer (δ_{Ro}) as the height of the peak value of Ro within the upper half of the domain. In Fig. 4e, we plot $\delta_{\text{Ro}}/\delta_{\nabla s}$, the ratio of these two boundary layers. As anticipated, the dynamical boundary layer (δ_{Ro}) becomes relatively thinner with respect to the thermal boundary layer ($\delta_{\nabla s}$) as Ro and \mathcal{P}_{Ro} decrease. [need a sentence saying what this means?]

4. DISCUSSION

In this letter, we studied low-Mach-number, stratified, compressible convection under the influence of ro-

tation. We examined three paths through Ra - Ta space, and showed that in the low- Ro , rotationally constrained regime, the newly-defined Predictive Rossby number, $\mathcal{P}_{\text{Ro}} = \text{Ra}/(\text{Pr Ta}^{3/4})$, determines the value of the evolved Ro . While increasing Ra and holding \mathcal{P}_{Ro} constant, we find scaling laws of heat transport (Nu) and turbulence (Re) that are nearly identical to scaling laws seen in nonrotational convection.

Our results here suggest that experimenters can achieve whatever degree of rotational constraint they desire in their evolved solution by choosing the proper value of \mathcal{P}_{Ro} . Once that value is chosen, traditional experiments in which the turbulent nature of the solutions is increased by increasing Ra can be straightforwardly achieved. While here we studied a simple cartesian geometry with antiparallel gravity and rotation, preliminary results in 3D spherical convective systems suggest that the results presented here are broadly applicable to rotational convection in complex geometries (Brown et al. 2019 in prep).

EHA acknowledges the support of NASA NESSF (insert fellowship number) and the University of Colorado’s George Ellery Hale Graduate Student Fellowship. This work was additionally supported by NASA LWS grant number NNX16AC92G. Computations were conducted with support by the NASA High End Computing (HEC) Program through the NASA Advanced Supercomputing (NAS) Division at Ames Research Center on Pleiades with allocations GID s1647.

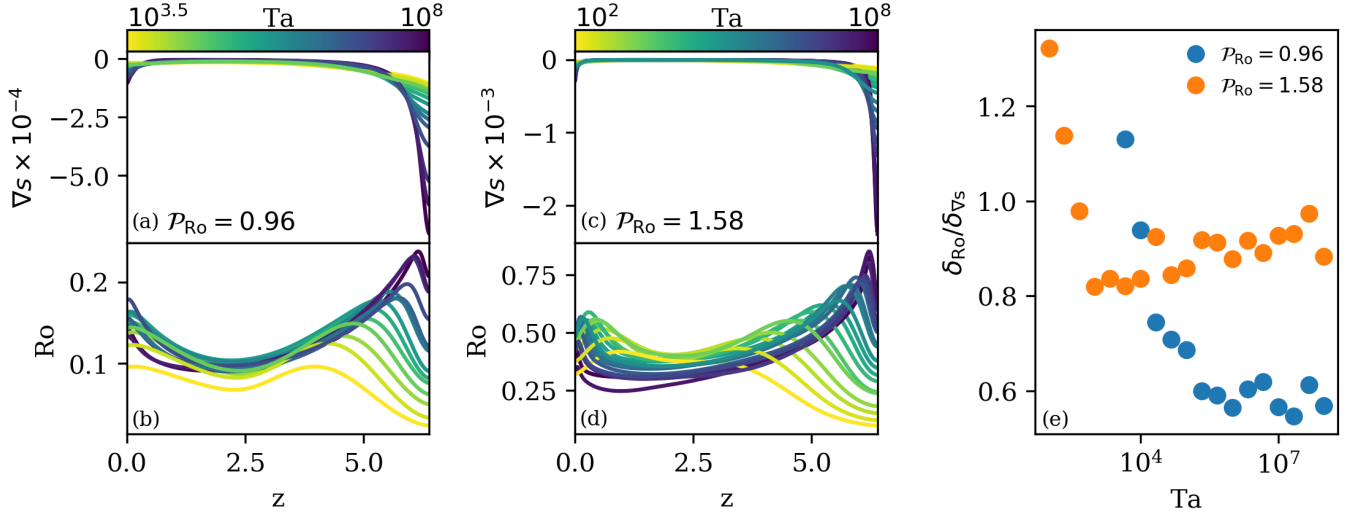


Figure 4. Horizontally-averaged profiles of the entropy gradient (∇s , a) and Rossby number (Ro , b) are shown vs. height for $P_{Ro} = 0.96$. Similar profiles are shown in (c) and (d) for $P_{Ro} = 1.58$. (e) The ratio of the sizes of the Ro boundary layer and ∇s boundary layer are shown. We find that for increasingly rotationally constrained flows, the Ro boundary layer is increasingly thinner than the thermal boundary layer.

REFERENCES

- Ahlers, G., Grossmann, S., & Lohse, D. 2009, *Rev. Mod. Phys.*, 81, 503
- Anders, E. H., & Brown, B. P. 2017, *Physical Review Fluids*, 2, 083501
- Augustson, K. C., Brown, B. P., Brun, A. S., Miesch, M. S., & Toomre, J. 2012, *ApJ*, 756, 169
- Aurnou, J. M., & King, E. M. 2017, *Proceedings of the Royal Society of London Series A*, 473, 20160731
- Brown, B. P., Browning, M. K., Brun, A. S., Miesch, M. S., & Toomre, J. 2008, *ApJ*, 689, 1354
- . 2010, *ApJ*, 711, 424
- Brown, B. P., Miesch, M. S., Browning, M. K., Brun, A. S., & Toomre, J. 2011, *ApJ*, 731, 69
- Brummell, N. H., Hurlburt, N. E., & Toomre, J. 1996, *ApJ*, 473, 494
- . 1998, *ApJ*, 493, 955
- Busse, F. H. 2002, *Physics of Fluids*, 14, 1301
- Calkins, M. A., Julien, K., & Marti, P. 2015, *Geophysical and Astrophysical Fluid Dynamics*, 109, 422
- Cheng, J. S., Stellmach, S., Ribeiro, A., et al. 2015, *Geophysical Journal International*, 201, 1
- Featherstone, N. A., & Hindman, B. W. 2016, *ApJ*, 830, L15
- Gastine, T., Wicht, J., & Aubert, J. 2016, *Journal of Fluid Mechanics*, 808, 690
- Glatzmaier, G. A., & Gilman, P. A. 1982, *ApJ*, 256, 316
- Greer, B. J., Hindman, B. W., & Toomre, J. 2016, *ApJ*, 824, 4
- Guerrero, G., Smolarkiewicz, P. K., Kosovichev, A. G., & Mansour, N. N. 2013, *ApJ*, 779, 176
- Julien, K., Knobloch, E., Rubio, A. M., & Vasil, G. M. 2012, *Physical Review Letters*, 109, 254503
- Julien, K., Legg, S., McWilliams, J., & Werne, J. 1996, *Journal of Fluid Mechanics*, 322, 243
- Käpylä, P. J., Käpylä, M. J., & Brandenburg, A. 2014, *A&A*, 570, A43
- King, E. M., Stellmach, S., Noir, J., Hansen, U., & Aurnou, J. M. 2009, *Nature*, 457, 301
- Soderlund, K. M., Sheyko, A., King, E. M., & Aurnou, J. M. 2015, *Progress in Earth and Planetary Science*, 2, 24
- Stellmach, S., Lischper, M., Julien, K., et al. 2014, *PhRvL*, 113, 254501
- Zhong, J.-Q., Stevens, R. J. A. M., Clercx, H. J. H., et al. 2009, *Physical Review Letters*, 102, 044502